THE JOURNAL OF PHYSICAL CHEMISTRY Letters

Cite This: J. Phys. Chem. Lett. 2018, 9, 3187−3192

Letter

pubs.acs.org/JPCL

Frequency-Swept Integrated and Stretched Solid Effect Dynamic Nuclear Polarization

T. V. Can,[†,‡] J. E. McKay,[§] R. T. Weber,[∥] C. Yang,[†,‡] T. Dubroca,[§] J. van Tol,[§] S. Hill,[§,⊥] and R. G. Griffin*[,†,‡]

[†]Francis Bitter Magnet Laboratory and [‡]Department of Chemistry, Massachusetts Institute of Technology, Cambridge, Massachusetts 02139, United States

[§]National High Magnetic Field Laboratory, Tallahassee, Florida 32310, United States

[∥]Bruker BioSpin Corporation, Billerica, Massachusetts 01821, United States

[⊥]Department of Physics, Florida State University, Tallahassee, Florida 32310, United States

ABSTRACT: We investigate a new time domain approach to dynamic nuclear polarization (DNP), the frequency-swept integrated solid effect (FS-ISE), utilizing a high power, broadband 94 GHz (3.35 T) pulse EPR spectrometer. The bandwidth of the spectrometer enabled measurement of the DNP Zeeman frequency/field profile that revealed two dominant polarization mechanisms, the expected ISE, and a recently observed mechanism, the stretched solid effect (S^2E). At 94 GHz, despite the limitations in the microwave chirp pulse length (10 μs) and the repetition rate (2 kHz), we obtained signal enhancements up to ∼70 for the S^2E and ∼50 for the ISE. The results successfully demonstrate the viability of the FS-ISE and S^2E DNP at a frequency 10 times higher than previous studies. Our results also suggest that these approaches are candidates for implementation at higher magnetic fields.

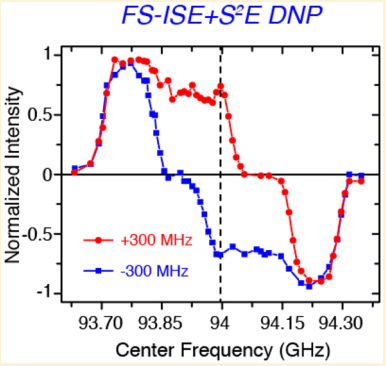

In a series of recent publications,[1−7] we explored time domain or pulsed dynamic nuclear polarization (DNP) experiments with the ultimate goal of enhancing the sensitivity of experiments in the rapidly expanding area of high field, DNP enhanced, magic angle spinning (MAS) NMR.[8−20] In particular, the primary motivation for developing time domain DNP is to circumvent the inverse field dependence of the signal enhancement observed with continuous-wave (CW) methods such as the solid and cross effects which scale as ω_0^{-n} where $n \sim 2$.[21,22] The challenge in performing these experiments is in generating and coherently controlling high power, high frequency microwave pulses. For example, the NOVEL experiment,[23,24] which is one of the most promising pulsed DNP experiments demonstrated to date, requires Rabi fields that match the condition $\omega_{1S} = \omega_{0I}$, where ω_{1S} and ω_{0I} are the electron Rabi and nuclear Larmor frequencies, respectively. Thus, at high magnetic fields used in contemporary MAS NMR experiments, it is necessary to employ high microwave powers to generate large electron Rabi frequencies. In order to circumvent this challenge, we initially performed experiments at 0.35 T that demonstrated the utility of an alternative approach to performing pulsed DNP, the frequency-swept version[7] of the integrated solid effect[24] (FS-ISE) and off-resonance NOVEL.[5] The advantage of these approaches is that the requisite electron Rabi frequency is much lower than that required to meet the NOVEL condition.

In the experiments described here, which explore the FS-ISE at 94 GHz/3.35 T, the ratio between the electron Rabi frequency and the ^{1}H Larmor frequency ω_{1S}/ω_{0I} was maintained constant at 30%, corresponding to less than 10% of the microwave power level required for NOVEL experiments. Our results at this frequency/field, which is a factor of 10 higher frequency than all other published pulsed DNP experiments, suggest that the FS-ISE is an excellent candidate for pulsed DNP at high fields. In addition, we have confirmed the presence of a recently observed mechanism, the stretched solid effect (S^2E), and provide a qualitative explanation for its origin. Finally, we have simulated the DNP field profile corresponding to both the FS-ISE and the S^2E.

Shown in Figure 1a is the echo detected EPR spectrum together with the solid effect (SE) DNP frequency profile. The experiments were performed on a sample consisting of 10 mM trityl-OX063 doped into a glycerol-d_8/D_2O/H_2O (60/30/10 volume ratio) glassy matrix at 80 K. The EPR spectrum exhibits a nearly Gaussian line shape but reveals a small anisotropy in the g-tensor of trityl-OX063. Using a train of microwave pulses at constant frequency, we recorded the DNP enhancement profile by incrementing the microwave frequency. This is essentially the SE DNP operating in pulsed mode, and the DNP enhancement profile consists of positive and negative peaks displaced from the EPR spectrum by the Larmor frequency of ^{1}H[21,25] at $\omega_{0S} \pm \omega_{0I}$, where ω_{0S} and ω_{0I} are the

Received: April 2, 2018
Accepted: May 14, 2018
Published: May 14, 2018

DOI: 10.1021/acs.jpclett.8b01002
J. Phys. Chem. Lett. 2018, 9, 3187−3192

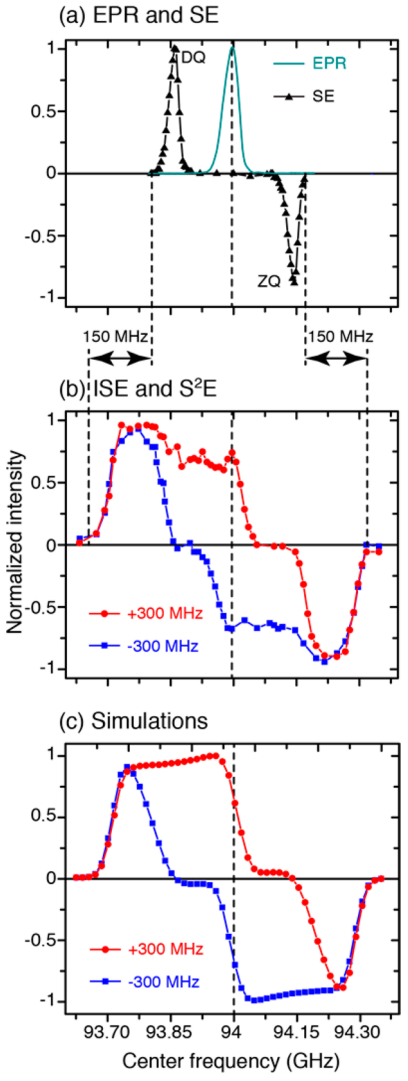

Figure 1. (a) Echo-detected EPR spectrum and SE enhancement profile (at incremented constant microwave frequencies). (b) ISE and S^2E enhancement profile with frequency sweep widths of +300 MHz (red) and −300 MHz (blue). Data were taken on a sample of glycerol-d_8/D_2O/H_2O (60/30/10 volume ratio) doped with 10 mM trityl-OX063 at 80K. The average microwave $\gamma B_1/2\pi$ was ∼40 MHz. The pulse length was 5 μs, and repetition rate was 1 kHz. Note that the edges of the profile in (b) are displaced by exactly half the sweep width (150 MHz vs 300 MHz). The maximum enhancements for the ISE and S^2E were ∼50 and 70, respectively, and were limited by the maximum in the contact time and the repetition rate (Figure 3). (c) Simulated DNP profiles using chirp microwave pulses with +300 MHz (red circles) and −300 MHz (blue squares) of sweep width. Simulations were performed for 3.35 T field, 3 μs microwave pulse length, 1 kHz repetition rate, and $\omega_{1S}/2\pi$ = 40 MHz. The time step was 0.1 ns during which the Hamiltonian is treated as time independent.

electron and ^1H Larmor frequencies, respectively. It is worth noting that the broad bandwidth of the spectrometer facilitates quick and automated acquisition of the enhancement profile by stepping the microwave frequency at constant B_0, thus circumventing the need to adjust RF tuning/matching at each nuclear Larmor frequency.

Shown in Figure 1b is the DNP frequency profile obtained using chirp microwave pulses of 5 μs pulse length applied at a 1 kHz repetition rate. During the chirp pulse, the microwave frequency was swept from $(\omega_c - (1/2)\Delta\omega)/2\pi$ to $(\omega_c + (1/2)\Delta\omega)/2\pi$, where $\omega_c/2\pi$ is the center frequency and $\Delta\omega/2\pi$ is the sweep width (SW). The SW of the chirp pulses was $\Delta\omega/2\pi = \pm$ 300 MHz, where the $\pm$ signs correspond to sweeping the frequency up/down from 150 MHz below/above to 150 MHz above/below with respect to the center frequency, respectively. The width of ±300 MHz was chosen based on the constraint that $|\Delta\omega| > 2\omega_{0I}$ is required to excite the ISE. The DNP profile was obtained by incrementing the center frequency ω_c of the chirp, and reveals two enhancement mechanisms: the intrinsic ISE and the stretched solid effect (S^2E). The ISE mechanism is dominant when the microwaves are on resonance with the EPR line of trityl, whereas the S^2E is broadened and displaced away from the SE shown in Figure 1a.

Figure 2 provides a semiquantative explanation for the three DNP mechanisms observed in the experimental data of Figure 1. Using monochromatic, off resonant microwave irradiation with an appropriate offset Ω to excite either the double quantum (DQ) or zero quantum (ZQ) transition results in the positive or negative SE, respectively (Figure 2a). Saturation of these transitions can also be achieved with chirped microwave pulses. In this case, a chirp with a SW of $\Delta\omega$ will excite the DQ or ZQ transition as long as the distance from its center frequency to the corresponding transition is smaller than $\Delta\omega/2$. This explains the broadening of the S^2E (Figures 1b) compared to the SE (Figures 1a). Furthermore, for $\Delta\omega > \omega_{0I}$, there exists a range of the center frequencies such that the chirp excites the EPR transition and then either the DQ or ZQ transition (but not both the DQ and ZQ). Excitation at the EPR transition in this case reduces the electron spin polarization, and thus attenuates or even eliminates the DNP enhancement. This explains the enhancement curve going to approximately zero at 94.1 GHz (red curve), and 93.9 GHz (blue curve) of Figures 1b. Correspondingly, the broadening of the S^2E peaks toward the center (EPR transition) is attenuated as opposed to broadening in the opposite direction. The latter is evident in the displacement by exactly $\Delta\omega/2$ of the edges of the S^2E compared to that of the SE (Figures 1b and 2b). This also explains the displacement of the peaks of the S^2E. At $\Delta\omega < \omega_{0I}$, Hovav et al.[26] showed that the S^2E is broadened equally in both directions, thus there is no displacement. In all cases, displacement of the edges provides a direct measurement of the SW. On the other hand, the correlation between the displacement of the S^2E peaks and the sweep width is more complicated.

The ISE dominates the enhancement process when the center microwave frequency is near the EPR transition and the SW is sufficiently broad to cover both the DQ and ZQ transitions (Figure 2c). Enhancements obtained at these transitions would have canceled one another if it were not for the electron spin inversion at the EPR transition. Furthermore, the sign of the ISE enhancement changes with the direction of the sweep, as opposed to the S^2E. Note that the sign of the ISE enhancement depends on whether the DQ or the ZQ transition is the first to be excited during the chirp: in particular, a chirp from low to high frequency (positive SW in our convention) would excite the DQ transition first, then the ZQ transition (Figure 1a) with an electron spin inversion in between, giving rise to positive enhancement. By contrast, similar to the SE, the S^2E relies on saturation of just one of the forbidden transitions, thus the direction of the chirp is irrelevant.

DOI: 10.1021/acs.jpclett.8b01002
J. Phys. Chem. Lett. 2018, 9, 3187−3192

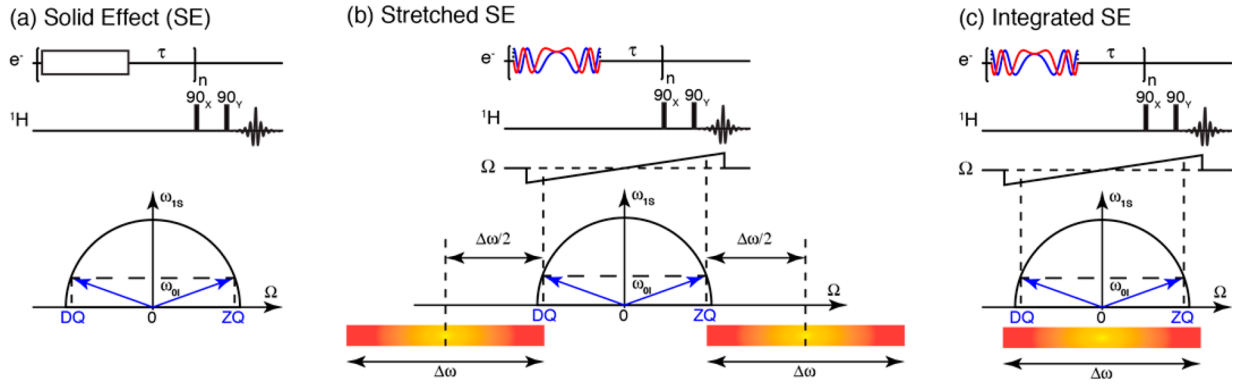

Figure 2. (a) Microwave irradiation at a fixed frequency leads to a positive SE if the offset is $\Omega = -\sqrt{\omega_{0I}^2 - \omega_{1S}^2} \approx -\omega_{0I}$ (DQ transition) or negative SE if $\Omega \approx +\omega_{0I}$ (ZQ transition). That relationship can be written as $\Omega^2 + \omega_{1S}^2 = \omega_{0I}^2$ and conveniently described by a semicircle of radius ω_{0I}.[24] (b) The DQ or ZQ transition can also be excited by a chirp microwave pulse with sweep width $\Delta\omega$ provided that the center frequency is in the range of $\pm\ \Delta\omega/2$ about the DQ or ZQ transitions, resulting in the broadening of the S^2E profile. When the center frequency is between the DQ or ZQ transitions, it is possible that the chirp will excite the EPR transition and either the DQ or ZQ transition, but not both. In such a situation, enhancement at the DQ or ZQ transition can be significantly reduced due to the saturation of the electron polarization at EPR transition; the resultant quenching leads to the appearance of shifts in the S^2E peak positions. (c) Chirp pulses with a center frequency near the EPR transition, and sweep width $\Delta\omega$ satisfying $\Delta\omega > 2\omega_{0I}$ lead to the ISE. A positive chirp (from low to high frequency) excites the DQ then the ZQ transition; the enhancements add in this case because of the electron spin inversion in between.

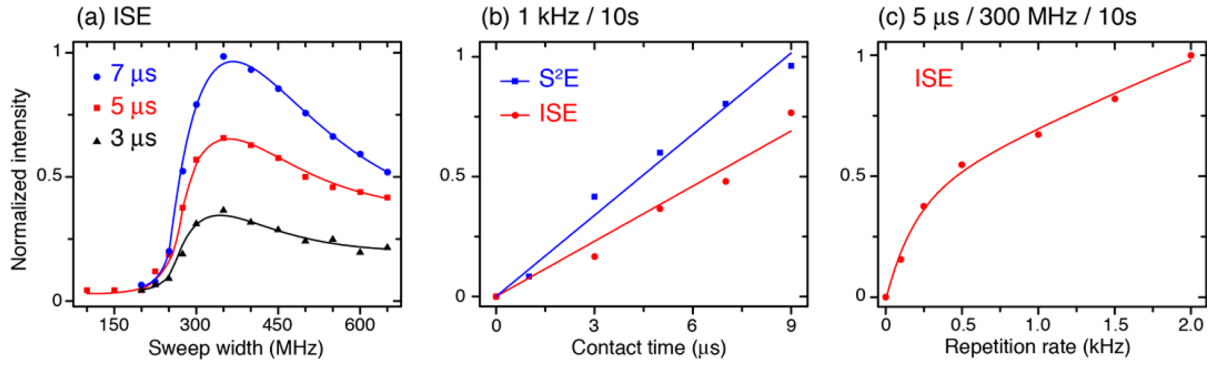

Figure 3. (a) ISE DNP enhancement as a function of the SW at different contact times of 3, 5, and 7 μs. Essentially no enhancement was obtained at a SW below 225 MHz because it is not broad enough to hit both the DQ and ZQ transitions, separated by twice the ^{1}H Larmor frequency (2 × 143 MHz) (Figure 1a). The optimum SW was ~350 MHz, which is enough to cover the entire SE field profile obtained with SW = 0 (Figure 1a). The enhancement decreases at broader SW. (b) Enhancement as a function of the contact time at a SW of 300 MHz. The enhancements obtained at both the ISE (center frequency of 94 GHz) and the S^2E+ (center frequency of 93.775 GHz) positions exhibit linear relationships and are far from saturation. (c) ISE enhancement as a function of repetition rate. The enhancement is still growing at the fastest repetition, which is currently limited by the power handling capability of isolators employed in the spectrometer.

The qualitative explanation of the field profiles in Figure 1 and pulse experiments in Figure 2 is further supported by quantum mechanical simulations using an in-house software package written in C++ (Figure 1c). Details of the implementation of this software package will be described elsewhere. Briefly, simulations were performed in the electron rotating frame of a 2-spin system consisting of a single electron and proton. Note that, in this frame, the Hamiltonian representing a chirp pulse is still time dependent, necessitating calculation of the propagator in a piecewise manner as described by Hovav et al.[26] The chirp pulses with SW of ±300 MHz were divided in time steps of 0.1 ns (30,000 steps for a 3 μs pulse). Calculations were performed in Liouville space to conveniently include the effect of relaxation via the superoperator formalism.[27,28] Although not completely quantitative, the simulations confirm the coexistence of ISE and S^2E in DNP experiments using chirp microwave pulses. Furthermore, important features of the DNP profiles were reproduced such as the broadening of the S^2E, the shifting of the S^2E peaks, and the existence of valleys in the profiles around 94.1 and 93.9 GHz. Overall, our simulations and experimental data are in excellent agreement.

As shown in Figure 3a, we did not observe any ISE enhancement when the sweep width is below ~250 MHz (±125 MHz about the EPR transition), because it is not sufficient to excite both the DQ and ZQ transitions of the SE frequency profile (Figure 1a) within the chirp bandwidth. The enhancement is optimized at a sweep width between 350 and 400 MHz. This is consistent with the fact that the sweep needs to cover the entire SE frequency profile in Figure 1a, which spans both the DQ and ZQ transitions that are separated by 286 MHz ($2 \cdot \omega_{0I}/2\pi$), as well as the full width of the EPR spectrum ($\delta \sim 80$ MHz). A broader sweep width attenuates the enhancement, probably because only the middle section of the pulse corresponding to a SW of ~350 MHz gives rise to DNP. This effectively shortens the pulse length. For instance, a 7 μs pulse with SW of ~500 MHz would be roughly equivalent to a ~5 μs pulse with SW of 350 MHz.

DOI: 10.1021/acs.jpclett.8b01002
J. Phys. Chem. Lett. 2018, 9, 3187−3192

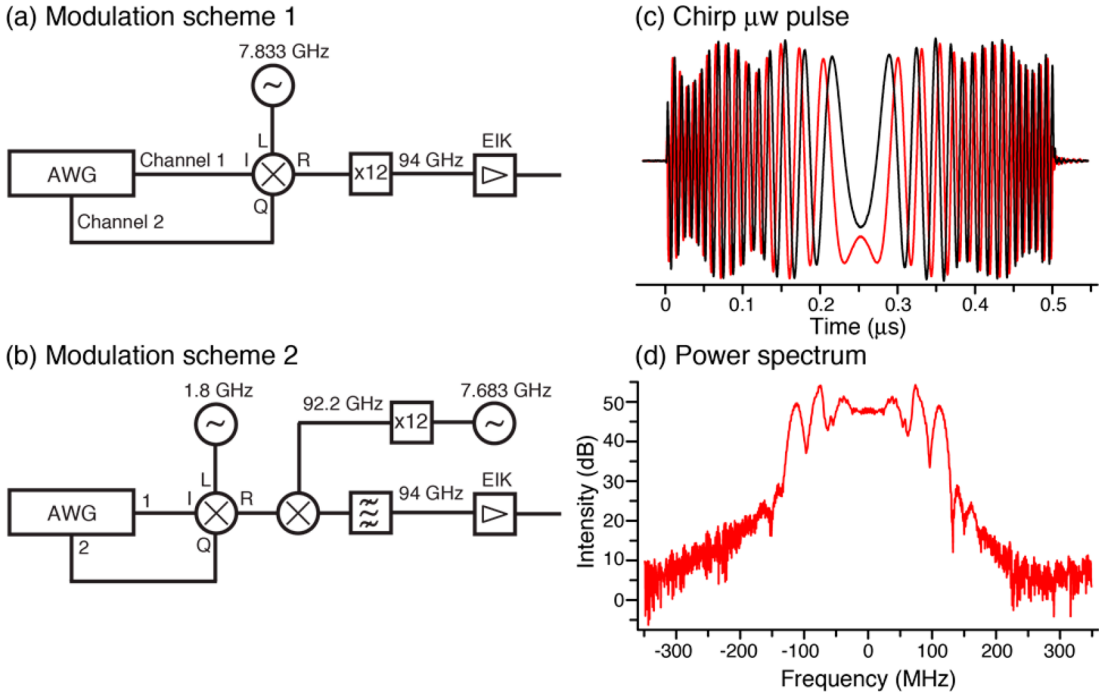

Figure 4. (a,b) Modulation of the microwave pulses at 94 GHz. In panel a, the pulses are first formed and modulated at 7.833 GHz by up-conversion mixing with signals from a 2-channel AWG using an IQ mixer operating at the LO frequency in 2−18 GHz range. The frequency was then multiplied by 12 to reach 94 GHz, followed by amplification by an EIK to obtained ∼1 kW output power at 94 GHz. The average $\gamma B_1/2\pi$ was ∼40 MHz. (c) An example of a chirp microwave pulse used in the ISE experiment. The sweep width was 250 MHz as seen in the corresponding power spectrum in panel d. The waveform at 94 GHz was recorded upon down mixing with a reference signal at 92.2 GHz.

Figure 3b,c illustrates the growth of the enhancement with increasing pulse length and repetition rate. At the longest pulse length and highest repetition rate, the enhancement is still not optimized at this microwave field strength. Nevertheless, we obtained enhancements of up to 70 for the S^2E and 50 for the ISE. The enhancements could be larger given more power or longer pulse lengths and higher repetition rates. The pulse lengths and repetition rates are currently limited by power handling limitations of isolators employed in the spectrometer (in principle, the EIK is capable of delivering an order of magnitude increase in average power). Despite operating below the optimum conditions, the enhancements obtained at 3.35 T are only about 2 to 4 times lower compared to the results at lower fields.

To fully employ the advantages of pulsed DNP, in particular the FS-ISE, requires high microwave fields ideally at or near the NOVEL condition. In our study, the microwave B_1 is ∼30% of the ^{1}H Larmor frequency and we found that, at this power level, the contact time needs to be quite long (Figure 3b). For DNP, one is not concerned with the dead time associated with the detection of EPR signals. Thus, a microwave cavity with a reasonable Q-factor could be employed to produce stronger Rabi fields that are closer to the NOVEL condition. However, the Q-factor cannot be too high because of the requirement of a broadband excitation for the FS-ISE sequence. Note that the sweep width is > $2\omega_{0I}$, thus the Q of the cavity should not be much larger than $\frac{\omega_{0S}}{2\omega_{0I}} \approx 330$. In fact, a Q-factor of just 10 is needed in the present case to reach the NOVEL condition, and future work will explore this possibility.

In summary, we have demonstrated the performance of pulsed DNP at the highest microwave frequency (94 GHz) and field strength possible at the present time (40 MHz or 30% of the Larmor frequency of ^{1}H). At this power level, the contact time for the FS-ISE sequence is long. Thus, the enhancements that we observed are limited by the microwave pulse length (10 μs) as well as the repetition rate (2 kHz). Nevertheless, enhancements up to 70 and 50 were obtained with the S^2E and FS-ISE, respectively. It is highly possible that these enhancements could become comparable to the results obtained at lower fields (9.5 and 34 GHz) with further refinement of the instrumentation. Our findings mark a major step toward pulsed DNP at high frequency and help guide further effort and strategy to perform these experiments at higher fields (>5 T).

EXPERIMENTAL METHODS

Experiments at 3.35 T (94 GHz/143 MHz electron and ^{1}H Larmor frequency, respectively) were performed at the National High Magnetic Field Laboratory (Tallahassee, Florida, USA). In particular, we employed the state-of-the-art high power pulsed EPR (HiPER) spectrometer with 1 kW of microwave power.[32,33] The microwave pulses were modulated at 7.833 GHz and converted to 94 GHz by a 12-fold frequency multiplier chain. At 94 GHz, the spectrometer can operate in either CW mode with ∼200 mW of power, or pulsed mode with 1 kW of peak power. In the pulsed mode of operation, the microwave power was amplified by an extended interaction klystron (EIK) amplifier with 60 dB of gain and a 1 GHz bandwidth.[32,33] For EPR detection an induction scheme is employed. The transmission and duplexing of the microwaves is achieved via a quasi-optical bridge. Isolation of the inductive mode EPR signal of interest is achieved by virtue of its detection in the orthogonal polarization with respect to the returning excitation pulse, which is coupled to the sample via a corrugated waveguide starting out at 50 mm inner diameter (ID) and tapering down to 3 mm ID. The sample holder is

DOI: 10.1021/acs.jpclett.8b01002
J. Phys. Chem. Lett. 2018, 9, 3187−3192

situated inside a customized (see below) 3 mm ID German silver waveguide. We note that this instrumentation does not currently employ a resonanator (i.e., $Q \sim 1$) in order to permit broadband excitation and short dead times needed for pulsed EPR experiments.

For NMR excitation and detection, the 3 mm ID waveguide was wrapped with a saddle coil (6 turns, 6 mm in diameter, 10 mm in length). The inductance of the coil was ~400 nH. The coil was electrically isolated from the German silver waveguide by a thin Macor sleeve (~1 mm thick). The standard metallic waveguide surrounding the sample holder effectively shields the RF field generated by the NMR coil. Therefore, this waveguide was modified by introducing slots by electrical discharge machining (EDM), similar to the structure used by Burghaus et al.[34] A ceramic capacitor of 2.7 pF (NP0 700 series from ATC) was soldered in parallel to the NMR coil. The resulting LC circuit (operating at 80 K) was connected to external tuning and matching capacitors (operating at room temperature) via a pair of semirigid coaxial cables to allow convenient adjustment of the RF resonance from outside the magnet.

Chirp modulation of the microwave frequency was achieved by a 2-channel arbitrary waveform generator (AWG) model DAx22000-8 M (Chase Scientific, Langley, WA 98260) with 2.5 GSa/s, 12-bit vertical resolution, and 8 MSa of memory per channel. The waveform from the AWG was mixed with the carrier frequency of 7.833 GHz using an IQ mixer (model MLIQ0218 from Marki Microwave) as shown in Figure 4a. The IQ mixing scheme allows for up-conversion of the carrier frequency by the AWG signals, generating exclusively the sum of the two frequencies. Frequency modulated pulses at 94 GHz were then obtained by a 12-fold frequency multiplier chain. Figure 4c features a typical chirp waveform at the input to the extended interaction klystron (EIK) amplifier that was down converted from 94 to 1.8 GHz for detection. Relatively minor imperfections in the waveform are believed to originate from modulation distortions arising in the x12 up-conversion scheme. However, one may ultimately expect a more uniform power spectrum than the one shown in Figure 4d at the output of the EIK due to saturation compression.

Besides the scheme shown in Figure 4a, it is also possible to perform the modulation directly at 94 GHz (Figure 4b) by mixing the 1.8 GHz AWG signal directly with a carrier frequency at 92.2 GHz. The output would include both the sum (94 GHz) and the difference (90.4 GHz) in this case. The low frequency component can be eliminated by a bandpass filter, an approach utilized by Guy et al.[29] This method of directly mixing the modulated waveform has the advantage of broader dynamic range and smaller error. However, the use of a frequency multiplier is more cost-effective in the present case. Furthermore, such a scheme is easier to implement at higher frequencies.[30,31] Direct modulation in the regime >200 GHz is not currently possible due to the paucity of microwave mixers and filters.

The T_1 of proton in the sample (glycerol-d_8/D_2O/H_2O 60/30/10 doped with 10 mM trityl-OX063) was 96 s at 80 K without microwave irradiation. Microwave irradiation at appropriate frequencies not only induces DNP but also shortens the buildup time T_B. For instance, at the ISE condition that gave an enhancement of 50, the T_B was 72 s. Due to the difference between T_1 and T_B, the enhancements were measured at $3T_1$ recovery time to ensure that both the DNP-enhanced and the Boltzmann signals reach their saturations. The value of n in Figure 2 is calculated accordingly. For example, during $3T_1$ (~300 s), the microwave pulse sequence was typically repeated at 1 kHz repetition rate, thus $n = 300 \times 1000 = 300\,000$.

AUTHOR INFORMATION

Corresponding Author

*E-mail: rgg@mit.edu.

ORCID

S. Hill: 0000-0001-6742-3620

R. G. Griffin: 0000-0003-1589-832X

Notes

The authors declare no competing financial interest.

ACKNOWLEDGMENTS

This research was supported by grants to R.G.G. from the National Institutes of Biomedical Imaging and Bioengineering, (EB-002804 and EB-002026), and by a grant to S.H. from the National Science Foundation (CHE-1229170). The 95 GHz experiments were performed at the National High Magnetic Field Laboratory, which is supported by National Science Foundation Cooperative Agreement No. DMR-1157490 and the State of Florida. We thank Peter Gorkov, Bianca Trociewitz, Ajay Thakkar, Jeff Bryant, and Qing Zhe Ni for their assistance.

REFERENCES

(1) Smith, A. A.; Corzilius, B.; Bryant, J.; DeRocher, R.; Woskov, P. P.; Temkin, R. J.; Griffin, R. G. A 140 GHz pulsed EPR/212 MHz NMR spectrometer for DNP studies. *J. Magn. Reson.* **2012**, *223*, 170−179.

(2) Smith, A. A.; Corzilius, B.; Haze, O.; Swager, T. M.; Griffin, R. G. Observation of strongly forbidden solid effect dynamic nuclear polarization transitions via electron-electron double resonance detected NMR. *J. Chem. Phys.* **2013**, *139*, 214201.

(3) Can, T. V.; Walish, J. J.; Swager, T. M.; Griffin, R. G. Time domain DNP with the NOVEL sequence. *J. Chem. Phys.* **2015**, *143*, 054201.

(4) Mathies, G.; Jain, S.; Reese, M.; Griffin, R. G. Pulsed Dynamic Nuclear Polarization with Trityl Radicals. *J. Phys. Chem. Lett.* **2016**, *7*, 111−116.

(5) Jain, S. K.; Mathies, G.; Griffin, R. G. Off Resonance NOVEL. *J. Chem. Phys.* **2017**, *147*, 164201.

(6) Can, T. V.; Weber, R. T.; Walish, J. J.; Swager, T. M.; Griffin, R. G. Ramped- amplitude NOVEL. *J. Chem. Phys.* **2017**, *146*, 154204.

(7) Can, T. V.; Weber, R. T.; Walish, J. J.; Swager, T. M.; Griffin, R. G. Frequency-Swept Integrated Solid Effect. *Angew. Chem., Int. Ed.* **2017**, *56*, 6744−6748.

(8) Mak-Jurkauskas, M. L.; Bajaj, V. S.; Hornstein, M. K.; Belenky, M.; Griffin, R. G.; Herzfeld, J. Gradual Winding of the Bacteriorhodopsin Chromophore in the First Half of Its Ion-Motive Photocycle: a Dynamic Nuclear Polarization Enhanced Solid State NMR Study. *Proc. Natl. Acad. Sci. U. S. A.* **2008**, *105*, 883−888.

(9) Bajaj, V. S.; Mak-Jurkauskas, M. L.; Belenky, M.; Herzfeld, J.; Griffin, R. G. Functional and shunt states of bacteriorhodopsin resolved by 250-GHz dynamic nuclear polarization-enhanced solid-state NMR. *Proc. Natl. Acad. Sci. U. S. A.* **2009**, *106*, 9244−49.

(10) Lesage, A.; Lelli, M.; Gajan, D.; Caporini, M. A.; Vitzthum, V.; Mieville, P.; Alauzun, J.; Roussey, A.; Thieuleux, C.; Mehdi, A.; Bodenhausen, G.; Coperet, C.; Emsley, L. Surface Enhanced NMR Spectroscopy by Dynamic Nuclear Polarization. *J. Am. Chem. Soc.* **2010**, *132*, 15459−15461.

(11) Rossini, A. J.; Zagdoun, A.; Hegner, F.; Schwarzwalder, M.; Gajan, D.; Coperet, C.; Lesage, A.; Emsley, L. Dynamic Nuclear Polarization NMR Spectroscopy of Microcrystalline Solids. *J. Am. Chem. Soc.* **2012**, *134*, 16899−16908.

(12) Gelis, I.; Vitzthum, V.; Dhimole, N.; Caporini, M. A.; Schedlbauer, A.; Carnevale, D.; Connell, S. R.; Fucini, P.;

DOI: 10.1021/acs.jpclett.8b01002
J. Phys. Chem. Lett. 2018, 9, 3187−3192

Bodenhausen, G. Solid-state NMR enhanced by dynamic nuclear polarization as a novel tool for ribosome structural biology. *J. Biomol. NMR* **2013**, *56*, 85−93.
(13) Fricke, P.; Demers, J. P.; Becker, S.; Lange, A. Studies on the MxiH Protein in T3SS Needles Using DNP-Enhanced ssNMR Spectroscopy. *ChemPhysChem* **2014**, *15*, 57−60.
(14) Becker-Baldus, J.; Bamann, C.; Saxena, K.; Gustmann, H.; Brown, L. J.; Brown, R. C. D.; Reiter, C.; Bamberg, E.; Wachtveitl, J.; Schwalbe, H.; Glaubitz, C. Enlightening the photoactive site of channelrhodopsin-2 by DNP-enhanced solid-state NMR spectroscopy. *Proc. Natl. Acad. Sci. U. S. A.* **2015**, *112*, 9896−9901.
(15) van der Cruijsen, E. A. W.; Koers, E. J.; Sauvee, C.; Hulse, R. E.; Weingarth, M.; Ouari, O.; Perozo, E.; Tordo, P.; Baldus, M. Biomolecular DNP-Supported NMR Spectroscopy using Site-Directed Spin Labeling. *Chem. - Eur. J.* **2015**, *21*, 12971−12977.
(16) Akbey, U.; Oschkinat, H. Structural biology applications of solid state MAS DNP NMR. *J. Magn. Reson.* **2016**, *269*, 213−224.
(17) Fricke, P.; Mance, D.; Chevelkov, V.; Giller, K.; Becker, S.; Baldus, M.; Lange, A. High resolution observed in 800 MHz DNP spectra of extremely rigid type III secretion needles. *J. Biomol. NMR* **2016**, *65*, 121−126.
(18) Lange, S.; Franks, W. T.; Rajagopalan, N.; Doring, K.; Geiger, M. A.; Linden, A.; van Rossum, B. J.; Kramer, G.; Bukau, B.; Oschkinat, H. Structural analysis of a signal peptide inside the ribosome tunnel by DNP MAS NMR. *Sci. Adv.* **2016**, *2*, e1600379.
(19) Mehler, M.; Eckert, C. E.; Leeder, A. J.; Kaur, J.; Fischer, T.; Kubatova, N.; Brown, L. J.; Brown, R. C. D.; Becker-Baldus, J.; Wachtveitl, J.; Glaubitz, C. Chromophore Distortions in Photointermediates of Proteorhodopsin Visualized by Dynamic Nuclear Polarization-Enhanced Solid-State NMR. *J. Am. Chem. Soc.* **2017**, *139*, 16143−16153.
(20) Wiegand, T.; Liao, W. C.; Ong, T. C.; Dapp, A.; Cadalbert, R.; Coperet, C.; Bockmann, A.; Meier, B. H. Protein-nucleotide contacts in motor proteins detected by DNP-enhanced solid-state NMR. *J. Biomol. NMR* **2017**, *69*, 157−164.
(21) Can, T. V.; Caporini, M. A.; Mentink-Vigier, F.; Corzilius, B.; Walish, J. J.; Rosay, M.; Maas, W. E.; Baldus, M.; Vega, S.; Swager, T. M.; Griffin, R. G. Overhauser effects in insulating solids. *J. Chem. Phys.* **2014**, *141*, 064202.
(22) Thankamony, A. S. L.; Wittmann, J. J.; Kaushik, M.; Corzilius, B. Dynamic nuclear polarization for sensitivity enhancement in modern solid-state NMR. *Prog. Nucl. Magn. Reson. Spectrosc.* **2017**, *102*, 120−195.
(23) Henstra, A.; Wenckebach, W. T. The theory of nuclear orientation via electron spin locking (NOVEL). *Mol. Phys.* **2008**, *106*, 859−871.
(24) Henstra, A.; Wenckebach, W. T. Dynamic nuclear polarisation via the integrated solid effect I: theory. *Mol. Phys.* **2014**, *112*, 1761−1772.
(25) Corzilius, B.; Smith, A. A.; Griffin, R. G. Solid effect in magic angle spinning dynamic nuclear polarization. *J. Chem. Phys.* **2012**, *137*, 054201.
(26) Hovav, Y.; Feintuch, A.; Vega, S.; Goldfarb, D. Dynamic nuclear polarization using frequency modulation at 3.34 T. *J. Magn. Reson.* **2014**, *238*, 94−105.
(27) Hovav, Y.; Feintuch, A.; Vega, S. Theoretical aspects of dynamic nuclear polarization in the solid state − The solid effect. *J. Magn. Reson.* **2010**, *207*, 176−189.
(28) Mentink-Vigier, F.; Akbey, U.; Oschkinat, H.; Vega, S.; Feintuch, A. Theoretical aspects of Magic Angle Spinning - Dynamic Nuclear Polarization. *J. Magn. Reson.* **2015**, *258*, 102−120.
(29) Guy, M. L.; Zhu, L.; Ramanathan, C. Design and characterization of a W-band system for modulated DNP experiments. *J. Magn. Reson.* **2015**, *261*, 11−18.
(30) Kaminker, I.; Barnes, R.; Han, S. Arbitrary waveform modulated pulse EPR at 200 GHz. *J. Magn. Reson.* **2017**, *279*, 81−90.
(31) Spindler, P. E.; Schops, P.; Kallies, W.; Glaser, S. J.; Prisner, T. F. Perspectives of shaped pulses for EPR spectroscopy. *J. Magn. Reson.* **2017**, *280*, 30−45.
(32) Cruickshank, P. A. S.; Bolton, D. R.; Robertson, D. A.; Hunter, R. I.; Wylde, R. J.; Smith, G. M. A kilowatt pulsed 94 GHz electron paramagnetic resonance spectrometer with high concentration sensitivity, high instantaneous bandwidth, and low dead time. *Rev. Sci. Instrum.* **2009**, *80*, 103102.
(33) Hunter, R. I.; Cruickshank, P. A. S.; Bolton, D. R.; Riedi, P. C.; Smith, G. M. High power pulsed dynamic nuclear polarisation at 94 GHz. *Phys. Chem. Chem. Phys.* **2010**, *12*, 5752−5756.
(34) Burghaus, O.; Rohrer, M.; Gotzinger, T.; Plato, M.; Mobius, K. A novel high-field/high-frequency EPR and ENDOR spectrometer operating at 3 mm wavelength. *Meas. Sci. Technol.* **1992**, *3*, 765−774.

DOI: 10.1021/acs.jpclett.8b01002
J. Phys. Chem. Lett. 2018, 9, 3187−3192